MAUSAM, 51, 4 (October 2000), 329-348

551.513.1 : 551.501.79(267)

On the semi-diagnostic computation of climatological circulation in the western tropical Indian Ocean

C. SHAJI, A.D. RAO and S.K. DUBE

Centre for Atmospheric Sciences,
Indian Institute of Technology, Hauz Khas, New Delhi – 110 016, India

and

N. BAHULAYAN

Physical Oceanography Division,
National Institute of Oceanography, Dona Paula, Goa – 403 004, India

(Received 30 September 1999)

सार — ग्रीष्म और शीत ऋतु के दौरान हिन्द महासागर के 20° दक्षिण के उत्तर में और 80° पूर्व के पश्चिम में मौसमी जलवायविक परिसंचरण माध्य का अन्वेषण त्रिविमीय, पूर्णतया अरैखिक अर्द्धडायगनॉस्टिक परिसंचरण मॉडल का उपयोग करते हुए किया गया है। इस मॉडल के समीकरणों में आधारभूत महासागरीय उष्णजलगतिक संवेग, द्रवस्थैतिक, सतता, समुद्र सतह बनावट और तापमान तथा लवण संवहन समीकरण सम्मिलित हैं। इस मॉडल में मौसमी सागर सतह वायु प्रतिवलन माध्य और विभिन्न स्तरों पर थर्मोहैलाइन आवेग के आँकड़ों के विषय में चर्चा की गई है। मॉडल का उपयोग करते हुए दो विपरीत ऋतुओं के दौरान महासागर की उपरी सतह की 20, 50, 150, 300, 500 और 1000 मीटर की गहराईयों पर उपरी सतहों के परिसंचरण ज्ञात किए गए हैं तथा पश्चिमी उष्णकटिबंधीय हिन्द महासागर में परिसंचरण के गतिकीय संतलन पर पवन के स्थानीय स्थायी आवेग और आंतरिक सघनता क्षेत्र की भूमिका की चर्चा की गई है। मॉडल को संचालित करने के लिए उपयोग किए गए जलवायविक तापमान और लवणता के आकड़े उपायोजन अवस्थाओं में सतह पवन, प्रवाह क्षेत्र और अधस्तल उच्चावच के साथ जलगतिकीय रूप से अनुकूल पाए गए हैं। जलवायविक तापमान और लवणता के आँकड़ों को अनुकूल बनाने के लिए और परिसंचरण के अनुकार मॉडलों में आरम्भिक स्थितियों के रूप में कार्य करने हेतु त्रिविमीय अपरिवर्ती अवस्था परिसंचरण को प्राप्त करने के लिए भी अर्द्धडॉयगनॉस्टिक नैदानिक तकनीक काफी प्रभावशाली सिद्ध हुई है।

ABSTRACT. The seasonal mean climatological circulation in the Indian Ocean north of 20°S and west of 80°E during the summer and winter has been investigated using a 3-dimensional, fully non-linear, semi-diagnostic circulation model. The model equations include the basic ocean hydrothermodynamic equations of momentum, hydrostatics, continuity, sea surface topography and temperature and salt transport equations. Model is driven with the seasonal mean data on wind stress at the ocean surface and thermohaline forcing at different levels. The circulation in the upper levels of the ocean at 20, 50, 150, 300, 500 and 1000 m depths during the two contrasting seasons has been obtained using the model, and the role of steady, local forcing of wind and internal density field on the dynamical balance of circulation in the western tropical Indian Ocean is explained. The climatological temperature and salinity data used to drive the model is found to be hydrodynamically adjusted with surface wind, flow field and bottom relief during the adaptation stages. Semi-diagnostic technique is found to be very effective for the smoothening of climatic temperature and salinity data and also to obtain the 3-dimensional steady state circulation, which would serve as initial condition in simulation models of circulation.

Key words —Semi-diagnostic model, 3-dimensional circulation, Sea surface topography, Thermohaline forcing, Steady state.

1. Introduction

The observed 3-D circulation in the monsoonal regions of Indian Ocean is controlled by local, unsteady and remote forcing, and it is essential to identify the role of each forcing on the observed circulation in the monsoonal area. The main local forcing to be considered in any mathematical model of

circulation of the tropical Indian Ocean are the surface wind, sea surface topography and variations in the internal density field. The semi-annual reversal of wind field generates large scale propagating signals such as Kelvin and Rossby waves that travel long distances to affect the ocean remotely (Luyten and Roemmiah 1982; Peregaud and Delecluse 1992). It is to be mentioned here that no single mathematical model of circulation can address all the above mentioned aspects, and it is essential that a hierarchy of mathematical models of circulation such as diagnostic, semi-diagnostic and prognostic are to be developed to identify the role of each of the above forcing on the observed circulation in the tropical Indian Ocean. The steady and transient responses of the tropical Indian Ocean have to be studied separately for a comprehensive understanding of circulation in this area.

The present study mainly addresses the role of steady, local forcing of wind, sea surface topography and internal density field on the dynamical balance of circulation in the western tropical Indian Ocean by using a semi-diagnostic circulation model. The concept and basic approach to semi-diagnostic modelling were first developed by Marchuk and Sarkisyan (1988). Some simplified semi-diagnostic models have been developed for other parts of the world oceans (Sarkisyan and Demin 1983; Marchuk and Sarkisyan 1988; Demin and Ibraev 1989). The model we have used is full depth with 33 levels at standard oceanographic depths and is driven by steady forcing of wind and internal density field. The climatological seasonal mean circulation for the summer and winter has been computed using the 33 level model. The model was driven with th4e climatology of Hellerman and Rosenstein(1983) wind field; the internal density field at various levels necessary to initialise the model were obtained from Levitus(1982) data on temperature and salinity. The adapted (steady state) results of currents, sea surface topography, temperature and salinity anomaly fields are presented in this paper. The computed results of surface currents are compared with climatological surface current compiled by Cutler and Swallow (1984) and other observations in the model area. The dynamics of computed currents in terms of local forcing considered in the model are also explained.

2. The semi-diagnostic circulation model

The model equations are based on the basic hydrothermodynamic equations that govern the large scale 3-dimensional flows in spherical co-ordinate system given by Gill (1982). Scale analysis of the governing equations shows that non-linear and friction terms have the same order of magnitude and both play a major role in the dynamics of circulation in the equatorial regions where geostrophy fails. The present model differs from the classical primitive equation models in two aspects: firstly, the model equations are written in terms of co-latitude of the place instead of usual latitutde and hence the Sine and Cosine functions of the model equations are modified; secondly, the spherical co-ordinate system used to write the model equations is different from the classical case in the sense that the meridional axis is taken positive towards south and the vertical axis is taken positive in the downward direction. Assuming approximations of Boussinesq, hydrostatics and incompressibility, the final model equations are written as follows :

The horizontal momentum equations are

$$\frac{\partial u}{\partial t} + Au + lv + \cot\theta \frac{uv}{R} = -\frac{1}{\rho_o R \sin\theta} \frac{\partial p}{\partial \lambda} + F^{\lambda} \quad (1)$$

$$\frac{\partial v}{\partial t} + Av - lu + \cot\theta \frac{u^2}{R} = -\frac{1}{\rho_o R} \frac{\partial p}{\partial \theta} + F^{\theta} \quad (2)$$

and the hydrostatic and continuity equations are

$$\frac{\partial p}{\partial z} = g\rho \quad (3)$$

$$\frac{1}{R\sin\theta}\left[\frac{\partial u}{\partial \lambda} + \frac{\partial (v\sin\theta)}{\partial \theta}\right] + \frac{\partial w}{\partial z} = 0 \quad (4)$$

Density of sea water is calculated from observations of temperature and salinity using the equation of state as

$$\rho = \rho(T, S) \quad (5)$$

The density of sea water 'ρ' is usually written in terms of another variable called sigma-t(σ_t) in the form as $\sigma_t = (\rho - 1)\ 1000$.

The temperature and salt diffusion equations are

$$\frac{\partial T}{\partial t} + AT = \frac{\partial \left[\nu_T \frac{\partial T}{\partial z}\right]}{\partial z} + \mu_T \Delta T \quad (6)$$

$$\frac{\partial S}{\partial t} + AS = \frac{\partial \left[\nu_T \frac{\partial S}{\partial z}\right]}{\partial z} + \mu_T \Delta S \quad (7)$$

In the above equations, θ is the co-latitude which is equal to 90-ϕ, ϕ is the latitude, u,v,w are the velocity components along the east(λ), south(θ) and downward(z) directions respectively; P is the hydrostatic pressure; ρ is the density of sea water which is taken as the sum of constant density ρ_o and density anomaly ρ', ρ_o is constant density which is equal to 1.0 gm cm^{-3}, R is radius of the Earth. $l=2\Omega\cos\theta$; Ω is angular velocity of Earth's rotation; A is advection operator, Δ is Laplacian operator, F^{λ}, F^{θ} are friction terms in the momentum equations; μ and ν are horizontal and vertical turbulent viscosity coefficients respectively; μ_T, ν_T are horizontal and vertical turbulent diffusion coefficients of heat and salt respectively; T is the temperature of sea water and S is the salinity of sea water.

$$Af = \frac{1}{R\sin\theta}\left[\frac{\partial(uf)}{\partial\lambda} + \nu\frac{\partial(f\sin\theta)}{\partial\theta}\right] + \frac{\partial(wf)}{\partial z}$$

$$F^{\lambda} = \frac{\partial\left(\nu\frac{\partial u}{\partial z}\right)}{\partial z} + \mu\left[\Delta u - \frac{u}{R^2\sin^2\theta} + \frac{2\cos\theta}{R^2\sin^2\theta}\frac{\partial v}{\partial\lambda}\right]$$

$$F^{\theta} = \frac{\partial\left(\nu\frac{\partial v}{\partial z}\right)}{\partial z} + \mu\left[\Delta v - \frac{v}{R^2\sin^2\theta} + \left(\frac{2\cos\theta}{R^2\sin^2\theta}\right)\frac{\partial u}{\partial\lambda}\right]$$

$$\Delta f = \frac{1}{R^2\sin^2\theta}\frac{\partial^2 f}{\partial\lambda^2} + \frac{1}{R^2\sin\theta}\frac{\partial\left(\sin\theta\frac{\partial f}{\partial\theta}\right)}{\partial\theta}$$

The density of sea water ρ is assumed to be the sum of a constant density ρ_o and density anomaly $\rho'(\lambda, \Theta, z)$. To calculate the pressure gradient terms in the equations (1) and (2), it is necessary to obtain the relation for hydrostatic pressure and the same can be obtained by integrating the hydrostatic equation (3) in the vertical from free surface to a depth z. Hence the expression for hydrostatic pressure at depth z cab be written as

$$P_z = g\,\rho_o\zeta + g\int_o^z \rho' dz \qquad (8)$$

In the above ζ is the sea surface topography or sea level. The pressure gradient terms in the momentum equations (1) and (2) are to be computed using equation (8). The unknowns in the model equations are the velocity components (u,v,w), density ρ, sea level ζ, temperature T and salinity S. It is, therefore, necessary to derive an additional expression for sea surface topography (sea level) to have a closed system of seven equations in seven unknowns. The procedure to derive the sea surface topography equation is given in the works of Bahulayan and Shaji (1996).

The eqns. (1)-(7), taking into account the equation for hydrostatic pressure (8) are solved with the help of a leap-frog numerical scheme. By assuming the equation of continuity along all levels taking into account the boundary condition at the surface and bottom for vertical velocity (*i.e.* w=0), the two dimensional integral continuity equation which is the equation for sea surface topography at the internal grid points is obtained. By applying the lateral boundary condition for velocity fields and substituting it in the two-dimensional integral continuity equation, the equation for sea surface topography at the boundary points are also obtained. The sea surface topography equation is solved by successive overrelaxation technique.

The model area lies between the latitudinal belt 30°N-20°S and longitudinal belt 35°E-80°E (Fig. 1). The entire southern boundary and part of the eastern boundary of the model are open boundaries where appropriate open boundary conditions for velocity or volume flux are to be specified. The western, northern and part of the eastern boundaries of the model are closed boundaries.

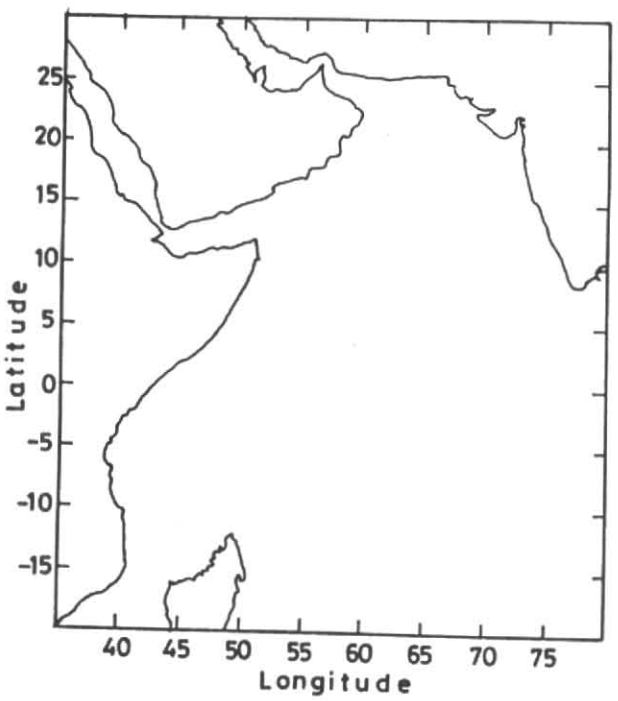

Fig. 1. Geometry of the model basin

At the surface (z=0), a rigid lid boundary condition for vertical velocity was employed. Specification of rigid lid boundary condition at surface will eliminate short period surface gravitational waves from the solution and it will enable us to use larger time steps of integration. However, large scale waves such as Rossby and Kelvin waves are retained in the solution. The resultant wind stress at the sea surface is expressed in terms of the gradient of velocity in the vertical multiplied by the vertical turbulent mixing coefficient and mean density of sea water. Thus, at the sea surface (z=0), the following boundary conditions are employed.

$$W|_{z=0} = 0 \qquad (9)$$

$$\rho_o\,\nu\frac{\partial u}{\partial z} = -\,\tau_\lambda\,;\ \rho_o\,\nu\frac{\partial v}{\partial z} = -\,\tau_\theta \qquad (10)$$

Where τ_λ and τ_θ are the components of wind stress in the zonal and meridional directions respectively and u,v are the components of velocity fields.

The boundary conditions for temperature and salinity are $T|_{z=0} = T^*;\ S|_{z=0} = S^*$ (11)

Where T^* and S^* are the observed temperature and salinity data at the surface.

At the bottom $z=H(\lambda,\Theta)$, non-slip boundary condition for velocity fields was applied.

$$i.e.\ u = v = w = 0 \tag{12}$$

For temperature and salinity, the following boundary conditions were used.

$$\frac{\partial T}{\partial \vec{n}} = \frac{\partial S}{\partial \vec{n}} = 0 \tag{13}$$

Where $\vec{n}$ is the normal to the sea bottom.

Along the rigid lateral boundaries of the model, the normal flux boundary conditions of zero velocity is prescribed.

$$i.e.\ \vec{V_n} = 0 \tag{14}$$

For temperature and salinity, we use the following boundary conditions:

$$\frac{\partial T}{\partial \vec{n}} = \frac{\partial S}{\partial \vec{n}} = 0 \tag{15}$$

Where $\vec{n}$ is the normal to the lateral boundary.

There are two open boundaries in the model area; the first zonal open sea boundary passes through 20°S latitude between the longitudes 35°E and 80°E and the second meridional open sea boundary passes along the longitude 80°E (Fig. 1). To conserve volume in the model area, the component of velocities or volume flux perpendicular to the open boundary should be balanced. In case the volume flux or the velocities are not balanced, appropriate corrections should be applied to the velocity fields at the boundary so that the velocities are balanced to the maximum extent possible.

If observed data on flow fields at certain stations along the open boundaries were available, those data could be interpolated to all the grid points along the boundary and such data are the best for the specifications of open boundary condition for velocity fields. Since current meter observations along the southern and eastern open boundaries were not available, it has become necessary to compute the flow field across the boundary by indirect method. There are a number of theoretical methods to compute the flow fields in the ocean and it is essential that the best method should be employed to obtain realistic values of current across the open boundaries. The theoretical method to compute the velocity fields should take into consideration the wind stress and thermohaline forcing. One of the drawbacks of geostrophic computation is that it computes only one component of the relative current that flows across the boundary. In addition, it also does not take into consideration the direct effect of wind stress which mainly control the surface circulation. In view of these drawbacks of geostrophic method, we have used a quasi- geostrophic model developed by Marchuk and Sarkisyan (1988) to compute the velocity components at various levels along the southern and eastern open sea boundaries. This model takes into consideration the wind stress, density field and sea level for the computation of velocity components.

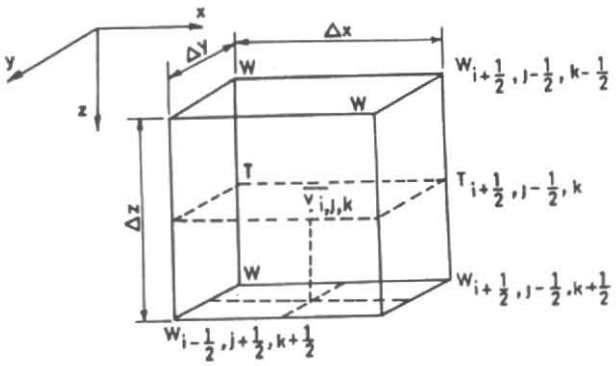

Fig. 2. A typical box in the finite-difference grid

An initial state of rest is given at time t=0 for the horizontal velocity components, and for the temperature and salinity data the observed values are prescribed.

$$(u, v)_{t=0} = 0 \tag{16}$$

$$(T, S)_{t=0} = (T^*, S^*) \tag{17}$$

The model equations (1-7) are solved subject to the boundary and initial conditions mentioned above using a leap-frog numerical scheme. While approximating the system (2.1 - 2.7) by finite difference technique, second order accuracy in spatial variables was achieved; the finite difference scheme also satisfies the main conservation laws that possess in the original system of equations. The model area was approximated by a set of boxes with equal horizontal axis, with velocity vector computed at its centre and the temperature and salinity computed at the lateral boundaries of the box as shown in Fig. 2. The vertical velocity is determined at equal distances between the nodal values T_k and T_{k+1} and the sea level is obtained at the sea surface z=0. While the coriolis term is treated in a semi-implicit fashion, the friction terms are calculated at the backward time level. All other terms in the equations are calculated at the central time level. To inhibit time-splitting instability normally encountered in the leap-frog scheme, a Matsuna scheme which averages solution at two consecutive time steps was employed at every 24 time steps.

In the semi-diagnostic method, the steady state solution of model equations is obtained in two stages on a 46×51 staggered grid. In the first stage, all the equations except turbulent diffusion equations of heat and salt are solved subject to proper boundary and initial conditions mentioned above. The integration of the equations is continued for approximately 30 days to obtain a quasi-steady solution for velocity field. The density is kept constant in this stage. In the second stage, the diagnostic equations together with the turbulent diffusion equations of heat and salt are again solved using the velocity field obtained during the first stage

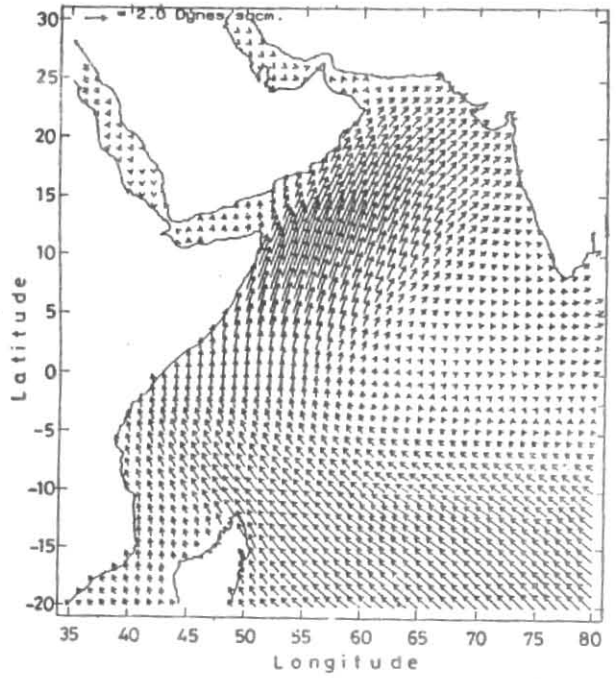

Fig. 3. Spatial distribution of mean resultant wind stress (dynes cm^{-2}) during summer season

and original temperature and salinity fields as initial conditions. The integration of the complete set of model equations is again continued for another 30 days to achieve a steady state solution. The total period of integration for both the stages is 60 days. A value of 5×10^8 cm^2 sec^{-1} is used for the horizontal eddy viscosity (μ) and eddy diffusivity (μt) coefficients in the model, whereas the vertical eddy viscosity (υ) and eddy diffusivity (υt) coefficients consider a value of 10 cm^2 sec^{-1}.

3. Results and discussion

The climatological wind data required to drive the model was obtained from Hellerman and Rosenstein (1983), the internal density field at various levels necessary to initialise the model was obtained from Levitus (1982) data on temperature and salinity. Brief descriptions of the forcing parameters such as wind field at the sea surface level and density (σ_t) at selected levels (6 levels) are given first before presenting the results on currents and sea surface topography. We strongly feel that presentation of the spatial variabilities of these forcing parameters would enable us to give meaningful interpretation to the results that were obtained from semi- diagnostic calculations.

3.1. *Summer season*

The summer mean wind stress (dynes cm^{-2}) for the model area that lies between the latitudinal belt 30°N - 20°S and longitudinal belt 35°E - 80°E is presented in Fig. 3. Strong southeasterly winds with magnitudes greater than 2.0

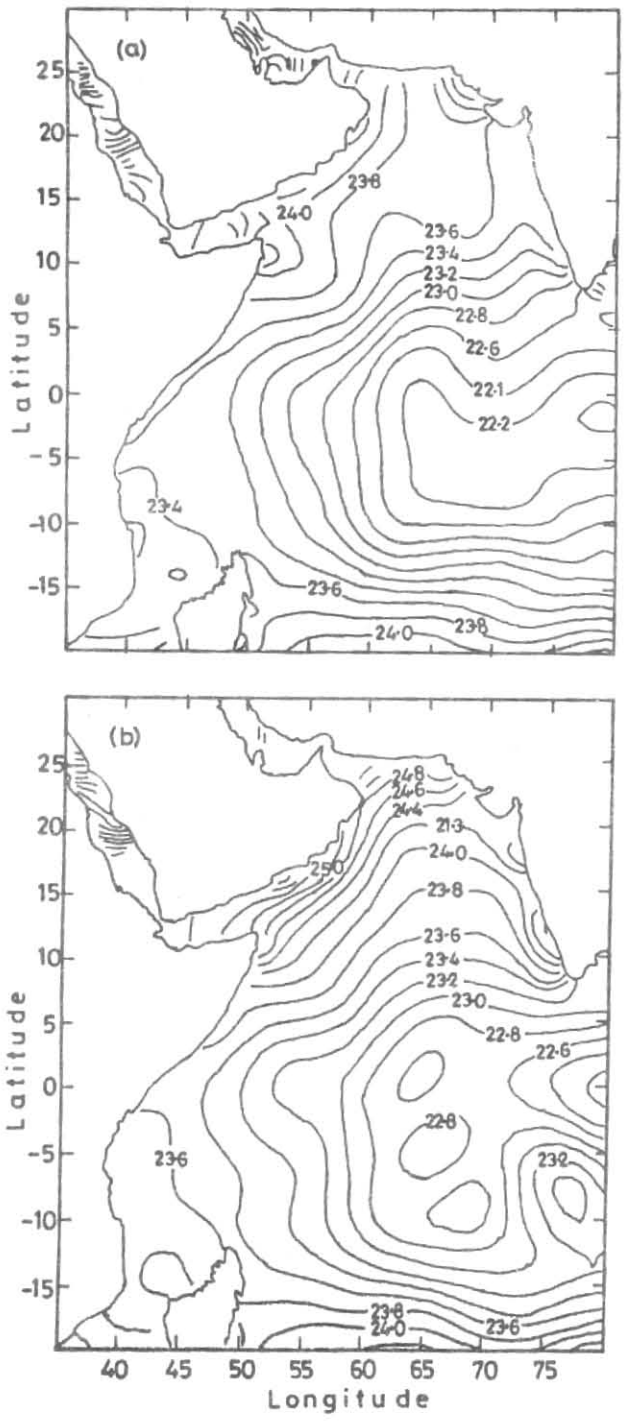

Figs. 4(a&b). Spatial distribution of σ_t fields during summer season at (a) 20 m depth and (b) 50 m depth

dynes cm^{-2} are observed during summer in the southern hemisphere between 10°S and 20°S latitude. These winds turn southerly on approaching the equator and then turn southwesterly after crossing the equator. Weak westerly winds prevail in the equatorial belt of the central Arabian

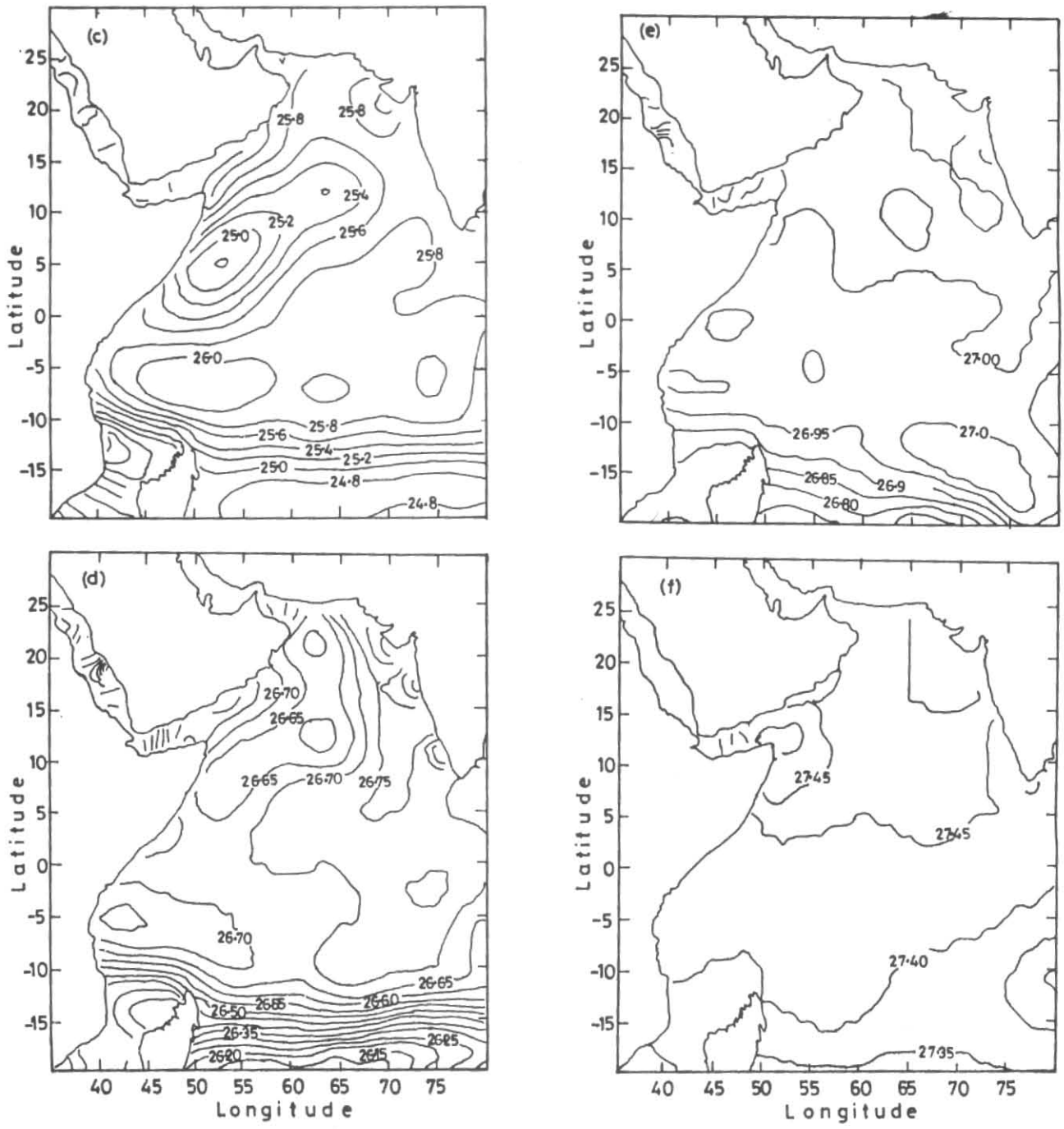

Figs.4 (c-f). Spatial distribution of σ_t fields during summer season at (c) 150 m depth (d) 300m depth (e) 500 m depth and (f) 1000 m depth

Sea between 5°N and equator. Southwesterly winds with magnitude greater than 2.0 dynes cm^{-2} are observed off Somali coast and in the northern Arabian Sea.

The mean sigma-*t* field during summer at 20, 50, 150, 300, 500 and 1000 m depths are presented in Figs. 4(a-f). At 20 m depth, between 20°S and equator, the σ_t values vary from 24.0 at 20°S to approximately 22.2 near the equator, and such kind of density distribution can generate a strong density driven westward current in this region. Off the Somali and Arabian coasts, σ_t values are fairly high because

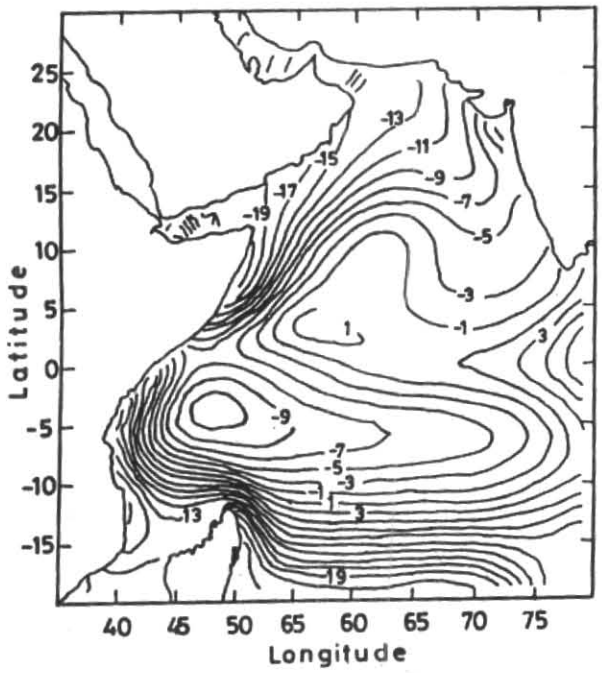

Fig. 5. Computed sea surface topography (cm) during summer season

of intense upwelling that takes place during the summer season. A zonal gradient in σ_t with maximum values in the western side, can be seen in the entire central and northern Arabian Sea. At 50 m depth, no significant change in σ_t distribution has been noticed in the South Equatorial Current region between 10°S and 20°S latitude. However, minor variations in σ_t has been noticed in the central and northern Arabian Sea. There is an increase in density in the northern extremity of Arabian Sea when compared to its distribution at 20 m depth.

At 150 m depth (Fig. 4c), significant changes in σ_t distribution have been noticed in the South Equatorial Current and Somali regions when compared to the distribution of σ_t at 20 and 50 m depths. The σ_t surface slopes downward from approximately 5°S to 20°S latitude; however, the gradient in the slope is not significant; the σt values range from approximately 26.0 at 5°S to 24.8 at 20°S latitude. Closed isolines of σ_t, indicating the presence of a large clockwise gyre, are noticed off the Somali and African coasts at 150 m depth. There is no significant variation in σ_t values in the central equatorial Indian Ocean and off the west coast of India.

At 300, 500 and 1000 m depths [Figs. 4(d-f)], the σ_t values are more smoothed with negligible gradient observed in the entire model area.

3.1.1. *Spatial variability of sea surface topography*

The sea surface topography is essentially controlled by the strength of the surface wind stress and interior flow fields that occur mainly in the thermocline region. In fact, the circulation in the thermocline region is mainly determined by the sea surface topography distribution. Oceanic motions occurring in the thermocline and above with spatial scales exceeding the Rossby radius of deformation will penetrate vertically to the surface and generate pressure signals which are reflected in the form of sea surface slope.

The mean sea surface topography during the summer season is presented in Fig. 5. The computed sea surface topography pattern shows the presence of a zonally oriented ridge extending all the way from the eastern part of the model area (80°E) to the East African coast between the latitudes 5°S and 20°S. The meridional sea surface gradient in these latitudes is found to be approximately 30 cm, and the highest sea level is located at the southern part of the model area. The sea surface topographic contours, which are heavily packed along the East African and Somali coasts, turn towards north and northeast on approaching the East African coast. The heavy packing of sea surface topographic contours indicates that the currents along the East African and Somali coasts are very strong. In the Arabian Sea north of equator, a zonal gradient in sea level, with the lowest along the Somali and Arabian coasts, has been observed and this zonal gradient is approximately of the order of 20 cm.

During the southwest monsoon season, four permanent surface currents are normally observed in the tropical Indian Ocean, and all these current systems could be seen from the sea surface topography pattern presented in Fig. 5. These four permanent currents are: (a) the westward flowing South Equatorial Current (SEC), located between the equator and 20°S latitude; (b) the northward flowing East African Coastal Current (EACC); (c) the northeastward flowing Somali Current (SC) and (d) the Southwest Monsoon Drift Current (SMDC) that encompass the entire Arabian Sea during the SW monsoon season.

The computed sea surface topography pattern could be explained in terms of the prevailing wind system and sigma-*t* distributioin in the model area. In the southern tropical Indian Ocean between the equator and 20°S latitude, winds are normally southeasterly and such wind system could induce an Ekman transport, which is perpendicular to the wind direction and to its left in the southern hemisphere. Waters in the upper levels are thus piled up against the southern boundary of the model area and this piling up of water would generate meridional gradient in sea level. The higher sea level observed off East African coast is also attributed to the piling up of sea water against the coasts due to Ekman transport. Along the Somali coast, the sea level is very much below the mean sea level and the same can be attributed to surface drift which is directed towards the right of the wind direction in the northern hemisphere.

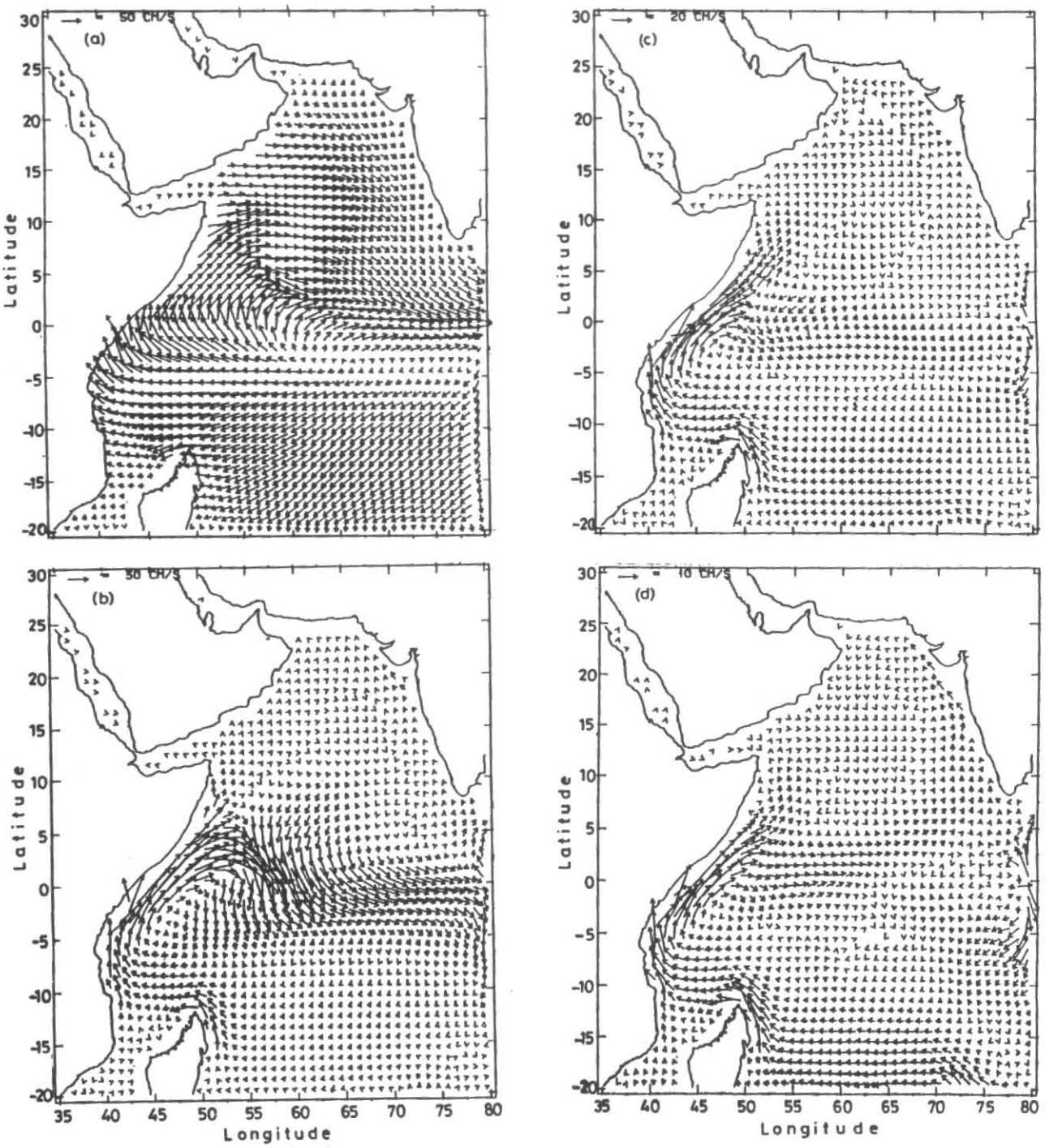

Figs. 6 (a-d). Computed currents (cm sec^{-1}) during summer season at (a) 20 m depth, (b) 50 m depth, (c) 150 m depth and (d) 300 m depth

3.1.2. *Spatial variability of currents at selected levels*

The computed currents at 20, 50, 150, 300, 500 and 1000 m depths are presented in Figs. 6 (a-f). The summer mean current pattern at 20 m depth (Fig. 6a) shows the presence of strong westward and southwestward flowing South Equatorial Current (SEC) in the entire southern tropical Indian Ocean between 5°S and 20°S latitude. This current (SEC) is mainly driven by the prevailing southeast trades which provide the major mechanical forcing for the basin-wide upper ocean circulation in the southern tropical Indian Ocean. The SEC is the most powerful, perennial current system in the southern tropical Indian Ocean. The computed SEC flows primarily toward the south of west, although zonal component could be seen in the northern

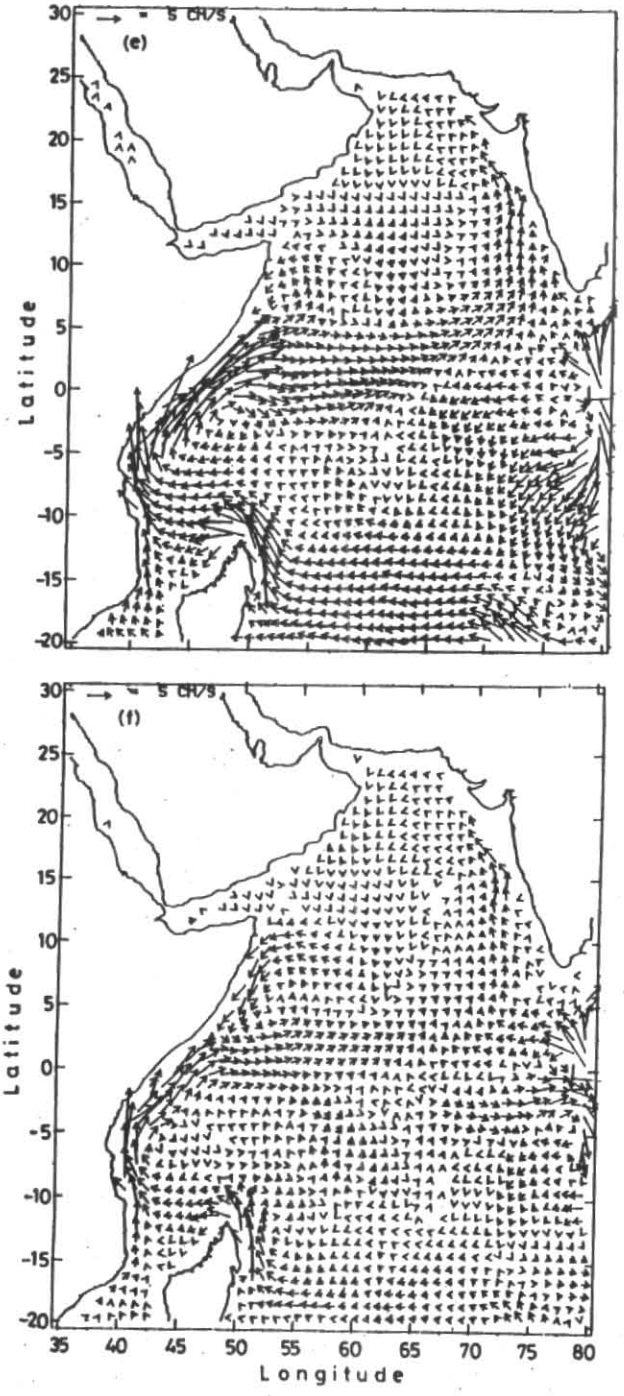

Figs.6 (e&f). Computed currents (cm sec^{-1}) during summer season at (e) 500 m depth and (f) 1000 m depths

portion of SEC. The magnitude of SEC varies between 50 cm sec^{-1} to 1 m sec^{-1}. The SEC, on reaching the East African coast, feeds initially the East African Coastal Current (EACC) and subsequently the northeastward flowing strong Somali Current (SC). The magnitude of Somali Current is approximately 1 m sec^{-1}. The Somali current turns eastward and southeastward at around 12°N latitude and feeds the

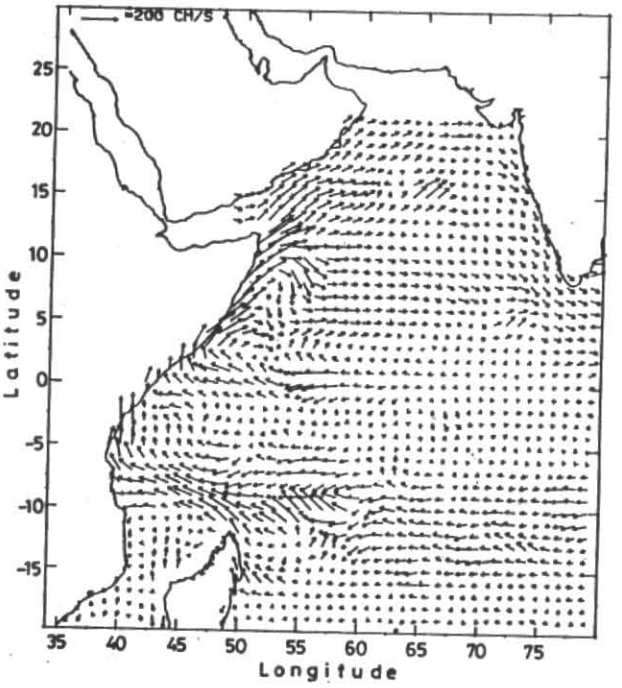

Fig. 7. The ship drift surface current of Cutler and Swallow (1984) during August

Southwest Monsoon Current (SWM). The SWM, which flows towards south of east, could be seen in the entire northern Arabian Sea. The winds during summer in the northern Arabian Sea are southewesterly and this would induce an Ekman drift current directed to the south of east. Primarily, the SWM is wind-driven, although the influence of density gradient on the strength and direction of flow could be seen to a lesser extent. The dynamical balance of this current will be discussed later after presenting the results of computed currents at other levels. The computed results at 20 m depth generally agree with the ship drift data compiled by Cutler and Swallow (1984) (Fig. 7). For a better comparison of model results with surface drift compiled by Cutler and Swallow(1984), the original ship drift climatology, compiled on a $2° \times 2°$ grid for each 10 day interval was first averaged for each month, and then the current field was interpolated to the model resolution of $1° \times 1°$ using cubic spline interpolation technique.

The summer mean current at 50 m depth is presented in Fig. 6(b). The circulation features at 50 m depth were significantly modified, both in terms of its magnitude and direction, *vis-a-vis* its features at 20 m depth. This is mainly due to the comparatively less role that wind plays on the circulation at subsurface levels. The circulation at the thermocline layers and below is mainly controlled by sea surface topography and vertical density variation. The SEC, which has become more zonal as compared to its pattern at the surface, flows westward between the latitudes 8°S and 20°S and turn towards north at the east coast of Madagascar. The

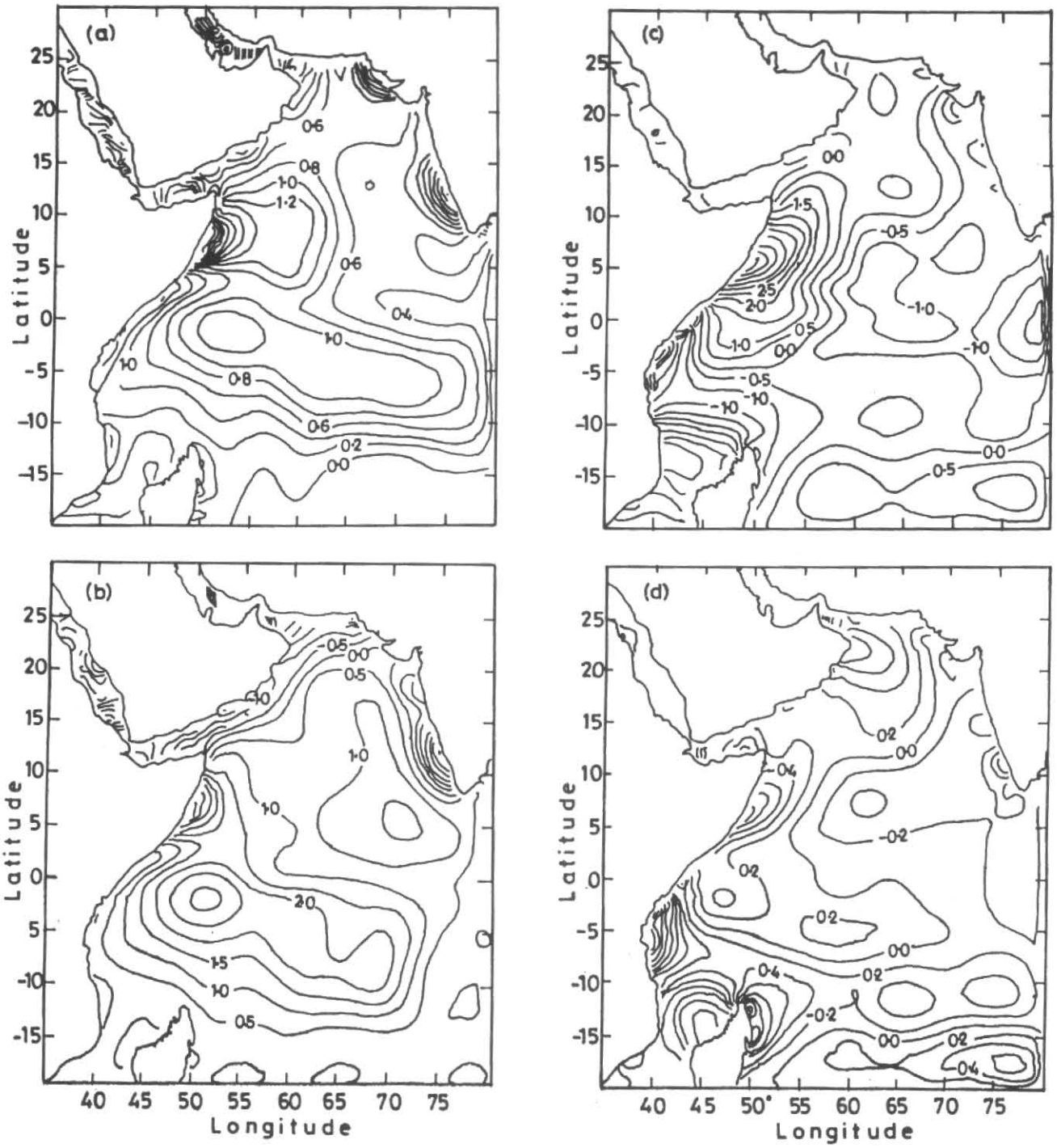

Figs. 8 (a-d). Temperature anomaly fields during summer at (a) 20 m depth, (b) 50 m depth, (c) 150 m depth and (d) 300 m depths

model could resolve only this northward flowing branch of SEC along the East Madagascar coast as the southern boundary of our model is located at 20°S latitude. Swallow *et al.* (1983) studied the boundary currents east and north of Madagascar using current measurements and temperature and salinity data and found that the SEC splits into two at approximately 17°S at the east coast of Madagascar. The southward flowing branch is called the East Madagascar Coastal Current (EMCC). The northward flowing coastal current along the east coast of Madagascar feeds into the northward flowing Somali Current (SC) *via* the East African Coastal Current (EACC), after travelling westward at the northern tip of Madagascar. The westward flow observed below the surface SEC is essentially a geostrophic flow,

caused by the balance of the steep meridional gradient in sea level and Coriolis parameter. Wyrtki (1973) observed the presence of westward flow below the surface SEC even upto 1000 m depth. Present model studies also support the findings of Wyrtki (1973).

Another important feature of circulation at 50 m depth is the presence of a strong eddy between 5°S and 5°N latitudes off the Somali region. This eddy which is normally seen in the Arabian Sea during the SW monsoon season, is caused by the peculiar sea surface topography distribution. The isolines of sea surface topography are closed in the entire equatorial regions between 35°E and 80°E and such sea surface topography distribution would drive a strong eastward flowing current between 5°N and 5°S. A strong zonal gradient in sea level, with the highest sea level at the western side of the basin, has been found in the equatorial belt, and such a zonal gradient in sea level could drive an eastward flowing current. In the northern Arabian Sea, the flow field is towards north and northeast all along the Arabian coasts, and it turns towards east and southward at the northern Arabian Sea at about 15°N latitude. This southward flowing current joins with the eastward flowing current between 5°N and 5°S. The computed circulation at 50 m depth is fully consistent with the sea surface topography distribution presented in Fig. 5. Another important feature of circulation at 50 m depth is the presence of a northward flowing coastal undercurrent all along the west coast of India. This coastal undercurrent could be seen only upto approximatelhy 300 km from the coastline, and is primarily a geostrophic current caused by the upward slope of the sea level towards the west coast of India. This northward flow turns towards south in the northern Arabian sea, and finally merges with the eastward flowing current located between 5°N and 5°S latitude.

The summer mean current at 150 and 300 m depths are presented in Figs. 6 (c & d) respectively. The circulation pattern at these two depths is not significantly different from what was observed at 50 m depth except that the magnitude of current is reduced and that the position of eddy located off Somali coast is shifted slightly towards south. The westward flowing subsurface SEC could be seen between 8°S and 20°S latitude. This SEC, after reaching the east coast of Madagascar, turn towards north and feeds the northward flowing Somali Current via the EACC. The clockwise eddy found off the Somali coast at 50 m depth is now shifted slightly towards south. This clockwise eddy is now located between the equator and 8°S latitude. The strength of the westward flowing SEC is approximately 10 cm sec^{-1}. The eastward flowing current that originates from approximately 50°E longitude could be seen between the latitudes 5°S and 2°N, and it continues upto the eastern part of the model area at 80°E longitude. The flow field is towards north and northeast all along the coasts of Somalia and Arabia, and it turns towards south at the northernmost extremity of Arabian Sea. The narrow northward flowing coastal undercurrent found along the west coast of India at 50 m depth is observed at 150 m depth also; however, its magnitude is slightly reduced which is of the order of 5 to 10 cm sec^{-1}. This northward coastal undercurrent that originates near the equator in the central part of the model area travels all the way upto the northern extremity of the Arabian Sea.

The summer mean current pattern at 300 m depth (Fig. 6d) is almost analogous to what is observed at 150 m depth, the only differnce being that the overall magnitude of the current is further reduced. The magnitude of current in the northern Arabian Sea is very less and it is approximately of the order of 5 cm sec^{-1}. The circulation pattern at 150 and 300 m depths are fully consistent with the sea surface topography pattern. The effect of horizontal variations in sigma-*t* is more than offset by the sea surface topography, and circulation essentially follows the sea level pattern.

The summer mean currents at 500 and 1000 m depths are presented in Figs. 6 (e & f) respectively. At both these depths, the northward flow along the west coast of India has become more broader and it now extends upto 5° from the coastline. A broad cyclonic gyre type of circulation was found in the northern Arabian Sea at both these depths. Another important feature of circulation along the Somali coast at 500 and 1000 m depths is that the flow is reversed, and a southward undercurrent is found all along the coastline from 10°N and the equator. This southward Somali undercurrent is mainly fed by waters from the Red Sea. The model studies by Jensen (1991) and current meter observations by Quadfasel and Schott (1983) reported the presence of southward flowing Somali undercurrent during August. The southward flow along the Somali coast meets the northward flow from the East African coast near the equator and both flows towards east as an undercurrent. This undercurrent could be seen upto the central part of Arabian Sea. The magnitude of currents at both these depths ranges between 2 cm sec^{-1} and 8 cm sec^{-1}. The eddy type of circulation, which was found off the east coast of Africa at 500 m depths, disappeared at 1000 m depth. The circulation pattern in the southern tropical Indian Ocean at 1000 m depth is more or less similar to what is observed at 500 m depth.

3.1.3. *Adjustment of temperature and salinity fields*

One of the main objectives of the semi-diagnostic modelling of circulation is to obtain, in addition to steady state circulation, hydrodynamically adjusted fields of temperature and salinity which could be used as the best initial fields in prognostic models of ocean circulation. The diagnostic calculation of currents suffers from two drawbacks:

(*i*) The available climatic temperature and salinity data contain high level "noise" effects of non-stationary processes.

(*ii*) The observed density field is not in adjustment with wind field and bottom relief of the ocean.

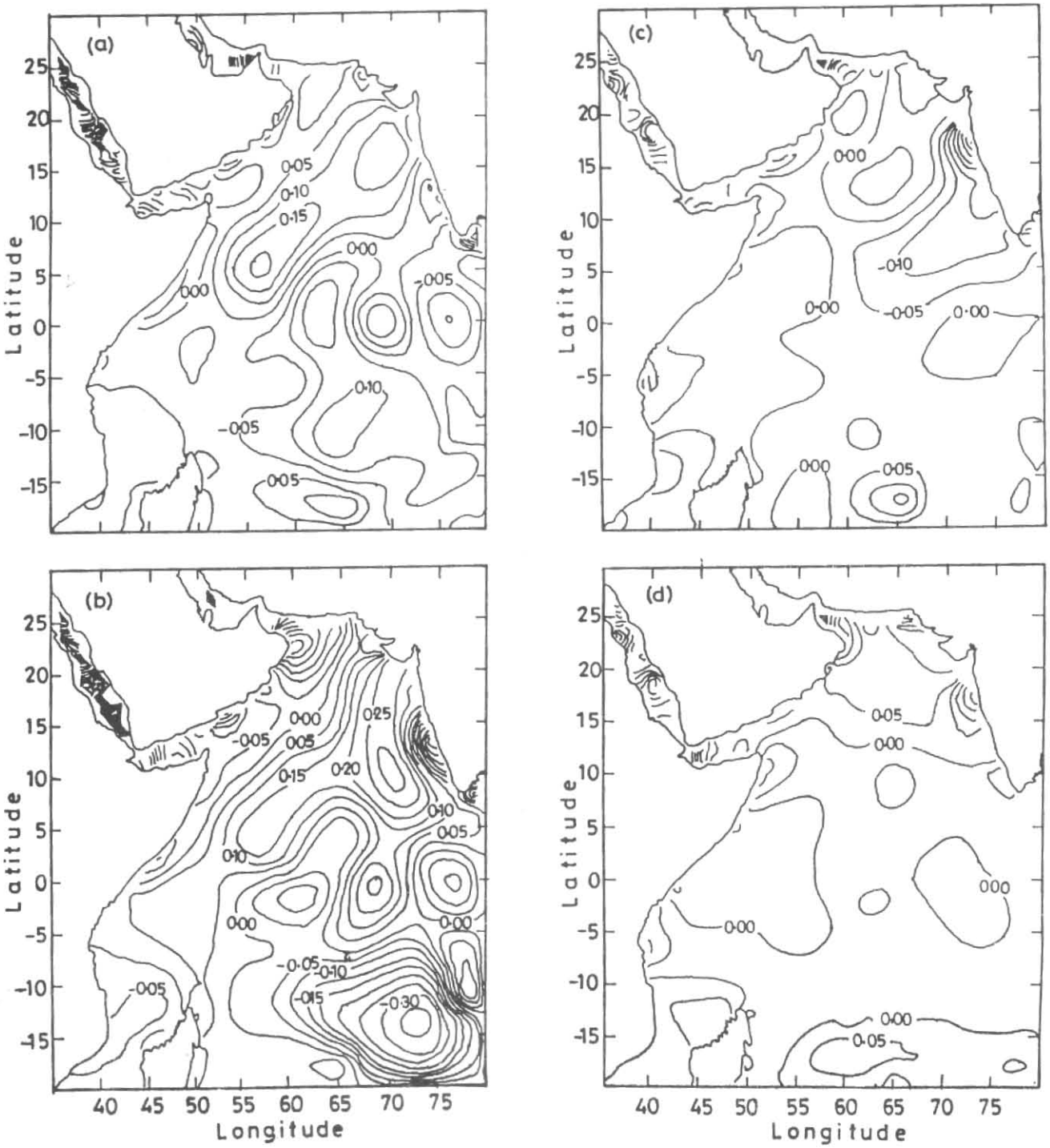

Figs. 9(a-d). Salinity anomaly fields during summer at (a) 20 m depth, (b) 50 m depth, (c)150 m depth and (d) 300 m depths

In view of the above, it is necessary to design models and to develop technique which would provide hydrological fields that are similar to observed data, and at the same time hydrodynamically adjusted without small scale "noises". The specified temperature and salinity data based on observations and the flow field calculated by diagnostic models are used as initial conditions in the semi-diagnostic model in which all the equations of motions including the equation of heat and salt are incorporated. The integration of the model equation continues only till the hydrological fields are adjusted with wind field and bottom relief. In our model studies, the specified temperature and salinity are hydrodynamically adjusted within 20 days of model integration from the diagnostic stage. The adjusted temperature and salinity

fields at selected depths are presented in the form of anomaly diagrams. The anomaly of a particular variable is equal to the difference between the observed variable and adjusted variable. During the adjustment stages, the input of temperature and salinity, which were given as initial conditions in the semi-diagnostic model, will have to deviate from its original values to a certain extent so that hydrodynamically adapted density and current fields free from "noises" are generated. If there is no deviations in the density field from its original values, the technique is not effective. The results presented in this section would show that semi-diagnostic technique is an effective tool for the initialisation of temperature and salinity data in simulation model of circulation.

The temperature and salinity anomaly fields at 20, 50, 150 and 300 m depths are presented in Figs. 8(a-d) & 9(a-d) respectively. Analysis of temperature anomaly fields at all the depths shows that the climatic temperature, which was used as initial condition in the semi-diagnostic model, was hydrodynamically smoothed (adjusted) during the adjustment process. In the southern tropical Indian Ocean south of 15°S latitude, the temperature anomaly field at 20 m depth is zero, indicating that there is no deviation between climatic temperature and adapted temperature. The temperature anomaly field increases slowly from 0.2°C at 15°S to approximately 1°C at the equatorial regions; the maximum anomaly of more than 2°C is noticed off the Somali coast which is the region of strong upwelling during the SW monsoon season. There is also a gradual increase in the temperature anomaly field from the west coast of India to the central part of Arabian Sea. at 50 m depth, negative temperature anomaly of 2°C was observed in the northernmost extremity of Arabina Sea. As noticed at 20 m depth, there is hardly any difference between the observed and adapted temperature at 50 m depth in the southern tropical Indian Ocean south of 15°S latitude; however, temperature anomaly increases slowly towards north and attains a value as high as 2.0°C in the equatorial regions. The temperature anomaly in the central Arabian Sea is of the order of approximately 1°C.

At 150 m depth, the maximum positive temperature anomaly is observed off the Somali coast where is value varies between 1°C and 4°C. Off the Mozambique and East African coasts, the temperature anomaly is negative, and the same negative temperature anomaly is noticed in the entire central and eastern Arabian Sea.

At 300 m depth, positive temperature amonaly of the order of 1°C was noticed in the northern extremity of Arabian Sea. Temperature anomaly varying between -0.2°C and -0.8°C was noticed in the entire eastern Arabian Sea. Positive temperature anomalies ranging between 0.2°C to 0.8°C could be seen off the Somali and African coasts.

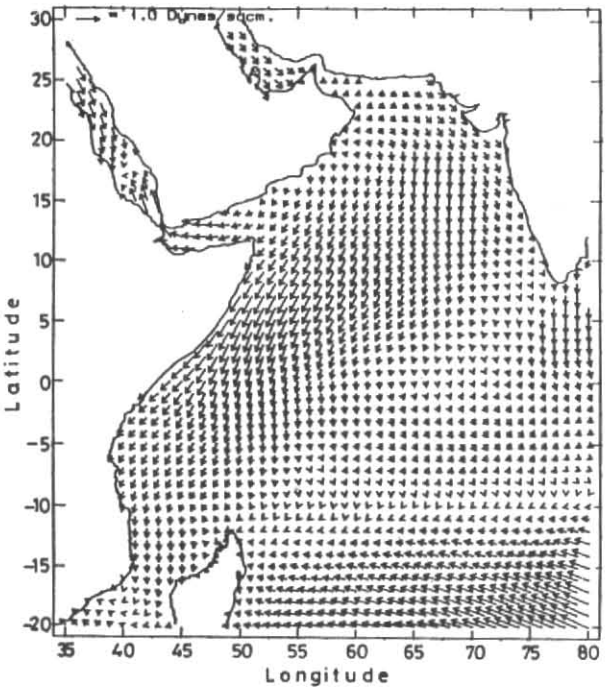

Fig. 10. Spatial distribution of mean resultant wind stress (dynes cm^{-2}) during winter season

The adapted salinity at 20 m depth shows that there is significant changes in the salinity values in the central Arabian Sea. The maximum positive salinity anomaly of 0.20 is noticed in the central Arabian Sea from where it decreases slowly towards the northern Arabian Sea. Negative salinity anomaly ranging between -0.05 to -1.00 could be seen in the entire eastern Arabian Sea and southern tropical Indian Ocean.

At 50 m depth, positive salinity anomaly ranging from 0.50 to 0.30 are observed in the northern Arabian Sea except the coastal regions of Arabia and northern Somalia. Maximum negative salinity anomaly of the order of 0.30 was observed in the southern tropical Indian Ocean. All along the coastal regions of Africa, negative salinity anomaly that ranges between 0.01 and 1.0 was noticed.

The summer salinity anomaly at 150 and 300 m depths are presented in Figs. 9(c & d) respectively. A comparison of the above two Figures shows that there is no significant salinity anomalies at greater depths. The salinity anomaly decreases with depth, indicating that the adaption technique not very effective at greater depths. At 300 m depth, the salinity anomaly is practically zero in the entire equatorial belt between 10°N and 10°S latitude. Positive salinity anomalies ranging from 0.05 to 0.15 are noticed in the northern Arabian Sea at 300 m depth.

3.2. *Winter season*

Before presenting the results of winter mean circulation and sea surface topography, we first give a brief description

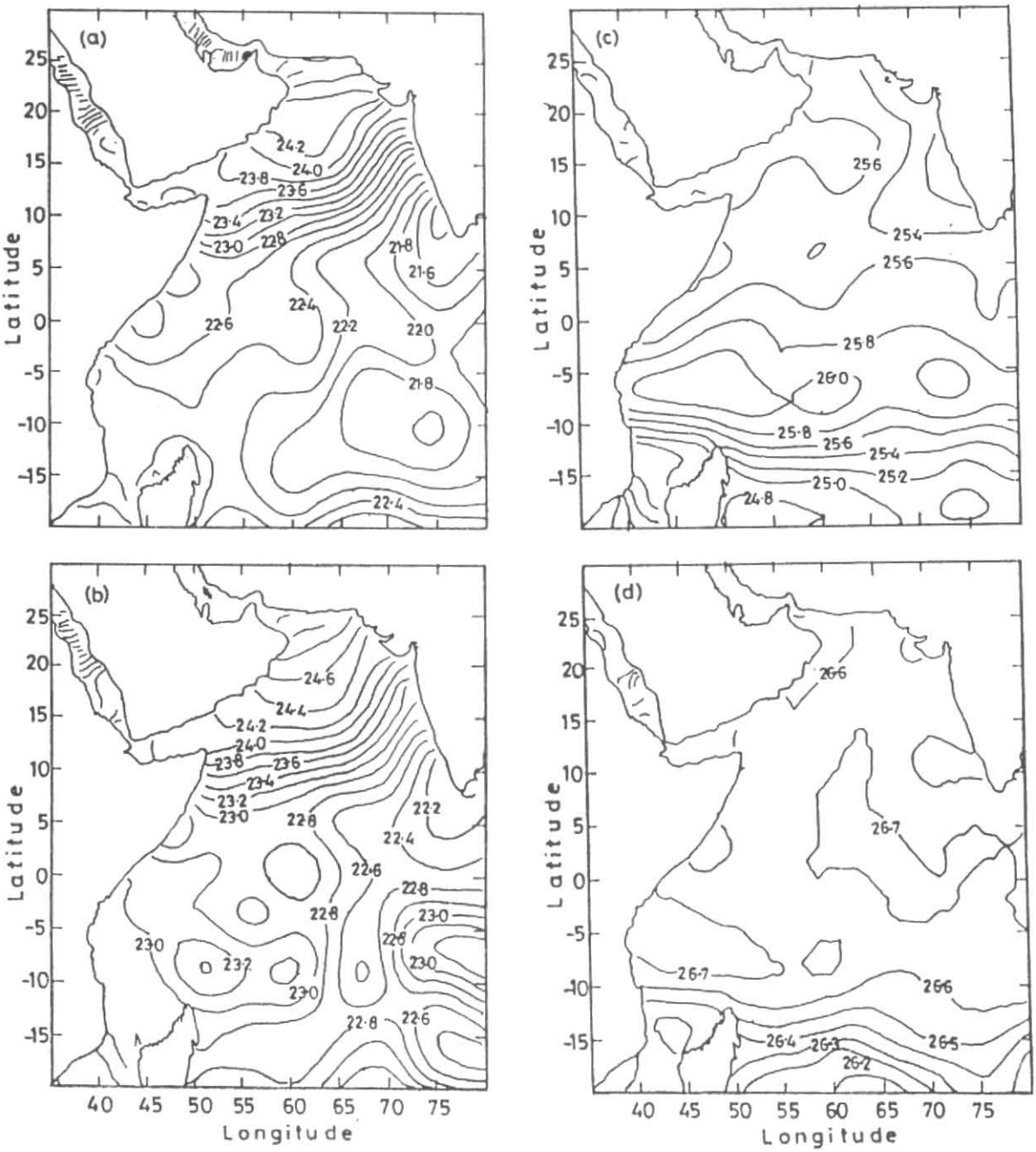

Figs. 11 (a-d). Spatial distribution of σ_t fields during winter season at (a) 20 m depth, (b) 50 m depth, (c) 150 m depth and (d) 300 m depth

of spatial distribution of forcing parameters of the model, namely the surface wind and density field (sigma-*t*) at selected levels.

The winter mean wind stress (dynes cm^{-2}) for the model area is presented in Fig. 10. The wind field is northwesterly all along the west coast of India and between the latitudinal belt 20°N-30°N. Northern and northeasterly winds could be seen in the Arabian Sea north of equator including the coastal regions of Africa. The strength of the northeasterly winds are high off the Somali region where its magnitude range between 0.5 and 1.0 dynes cm^{-2}. In the southern tropical Indian Ocean south of 10°S latitude, strong south-

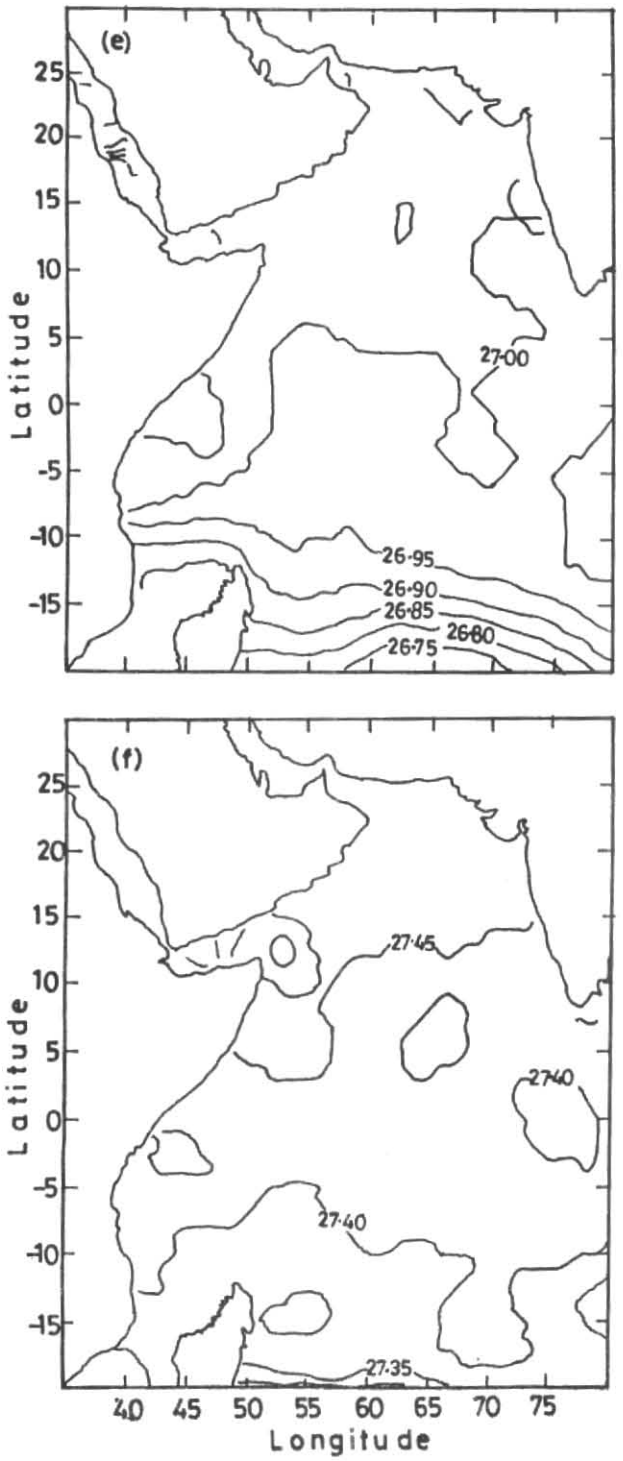

Figs. 11 (e&f). Spectral distrubution of σ_t fields during winter at (e) 500 m depth and (f) 1000 m depth

easterly and easterly winds could be seen; however, winds are very weak in the equatorial Indian Ocean east of 50°E *longitude.*

The mean σ_t(sigma-*t*) field during winter at 20, 50, 150, 300, 500 and 1000 m depths are presented in Figs. 11(a-f). At 20 m depth, the σ_t decreases from 22.6 at 20°S to approximately 21.8 at 5°S latitude, there is no significant variation in σ_t in the equatorial regions between 5°N and 5°S. North of 5°N latitude, the σ_t increases towards north, and at the northern extremity of Arabian Sea, the observed σ_t is approximately of the order of 24.8. The σ_t lines are oriented in a southwest-northeast direction in the entire Arabian Sea north of 5°N at 20 m depth.

At 50 m depth, the σ_t surface slopes downward from 5°S to 20°S in general, except the eastern part where small cells of high density water masses could be seen. In the equatorial regions between 5°N and 5°S, a zonal gradient in density field, which could generate an eastward density driven flow extending upto the eastern boundary of the model area, is observed. As noted at 20 m depth, the σ_t at 50 m depth increases towards north from 5°N latitude, and at the northern extremity of the Arabian Sea,the oserved σ_t is approximately of the order of 25.0. The orientation of σ_t lines in this region is almost analogous to what is observed at 20 m depth.

The σ_t distribution pattern at 150, 300, 500 and 1000 m depths are entirely different from what is observed at 20 and 50 m depths. The σ_t lines are oriented in a zonal direction at all these depths in the southern tropical Indian Ocean: in addition, the meridional gradient in density is also decreased. No significant variation in σ_t has been noted in the entire northern Arabian Sea at the above mentioned depths.

3.2.1. *Spatial variability of sea surface topography*

The mean sea surface topography during the winter is presented in Fig. 12. As observed in the summer, the computed sea surface topography during winter also shows the presence of a zonally oriented sea surface topography ridge between 10°S and 20°S latitude. The meridional sea surface gradient between these latitudes is found to be approximately 35 cm, and the highest sea level is located at the southern part of the model area. There is no significant variations in the sea surface topography pattern in the meridional direction between the latitudes 10°S and 5°N; however, a zonal gradient in sea level with higher levels at the western side was noticed in the equatorial regions. Small circular topographic troughs and ridges are also found in the equatorial Indian Ocean. In the northern Arabian Sea north of 12°N, the sea level slopes downwards in general.

The computed sea surface topography pattern could be explained in terms of both the prevailing wind systems and the density distribution in the area. In the southern tropical Indian Ocean between 10°S and 20°S latitude, the winds are generally southeasterly and easterly; such wind system would induce Ekman transport and Ekman drift to the left to its direction in the southern hemisphere, leading to the

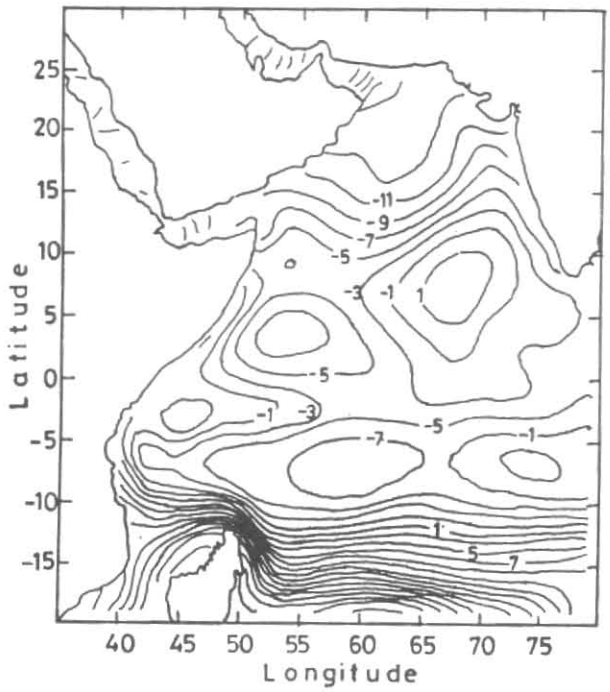

Fig. 12. Computed sea surface topography (cm) during winter season

piling up of sea water against the southern boundary of the model area. This piling up of water would generate meridional gradient in sea level. The density of water along this belt is also low as compared to other regions, and this low density distribution would additionally contribute for the increase of sea level at the southern boundary of the model area. The higher density observed in the northernmost extremity of the Arabian Sea, coupled with the southward and southwestward drift of water in response to northerly winds, are responsible for the generation of meridional gradient in sea level in the northern Arabian Sea.

3.2.2. *Spatial variability of currents at selected levels*

The computed winter mean currents at 20, 50, 150, 300, 500 and 1000 m depths are presented in Figs. 13(a-f).

The winter mean current pattern at 20 m depth shows the presence of a strong southwestward flowing South Equatorial Current (SEC) in the entire southern tropical Indian Ocean between 10°S and 20°S latitude. This current is mainly driven by the prevailing southeast trades which provide the main mechanical forcing for the basin wide circulation in the southern tropical Indian Ocean. The computed SEC flows primarily toward the south of west during winter mainly because the prevailing wind systems are easterly and southeasterly in the entire domain. The magnitude of SEC during winter is weak as compared to summer season and it varies between 30 cm sec^{-1} to 20 cm sec^{-1}. Part of SEC on reaching the East Madagascar coast turns towards north along the coast and joins with the East African Coastal Current (EACC). The EACC joins with the southward flowing Somali Current (SC) between the equator and 5°S latitude, and both jointly feed the strong eastward flowing Equatorial Counter Current (ECC) that flows between the equator and 10°S latitude. The North Equatorial Current (NEC) is present in the computed results between 10°N and equator. North of 10°N, the currents are westward throughout the Arabian Sea and it is driven by the prevailing wind systems which are either notherly or northeasterly during winter.

In general, the entire current systems at 20 m depth are primarily driven by the prevailing wind systems. The model has been successful in reproducing all the permanent current systems in the western tropical Indian Ocean during the winter season (Fig. 14); however, the northward flow observed along the southwest coast of India during winter is not reproduced by the model. The present model does not consider the remote forcing from the Bay of Bengal which are mainly responsible for the northward flow along the southwest coast of India during the winter season (McCreary *et al.* 1993). The eastern boundary of our model is open where zero balance in velocities are maintained throughout the model integration to conserve volume and hence the effect of Bay of Bengal could not be studied in the

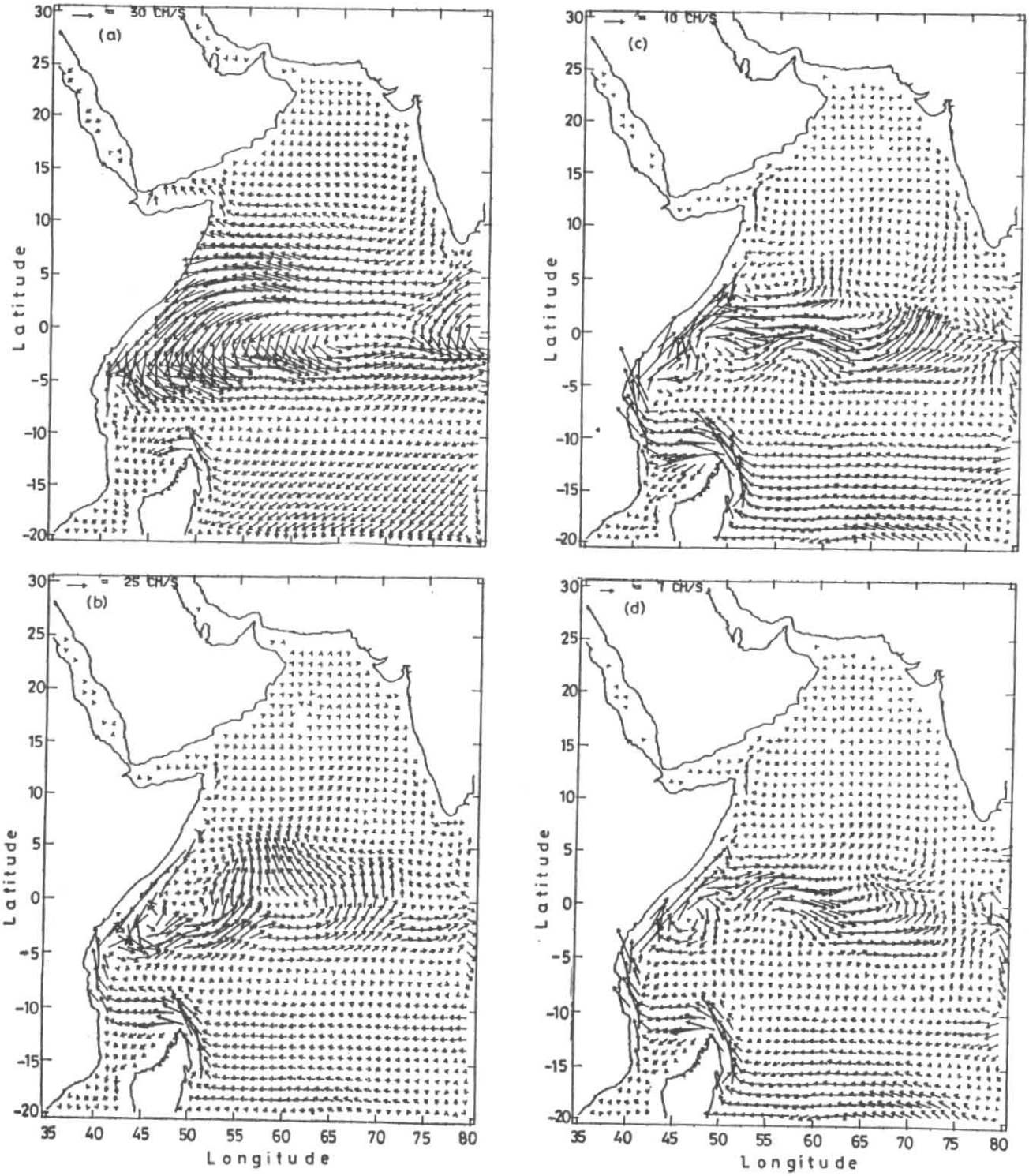

Figs. 13(a-d). Computed currents (cm sec^{-1}) during winter season at (a) 20 m depth, (b) 50 m depth, (c) 150 m depth and (d) 300 m depth

present model study. Our model studies also indirectly support McCreary's findings (McCreary *et al.* 1993) that remote forcing from the Bay of Bengal are responsible for the northward flow along the southwest coast of India.

The circulation patterns at 50m depth (Fig. 13b) are significantly modified, both in terms of magnitude and direction, *vis-a-vis* its features at 20 m depth, mainly because of comparatively less role that wind plays on the circulation

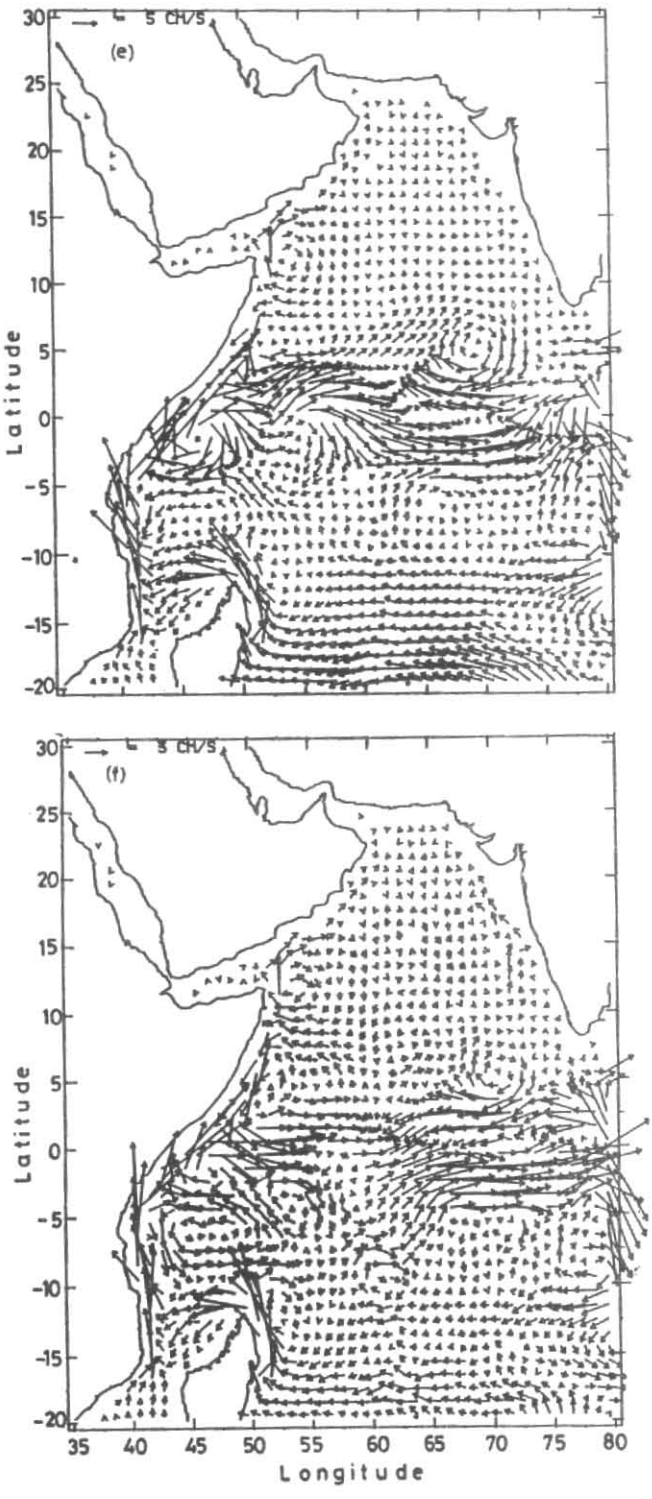

Figs. 13 (e&f). Computed currents (cm sec^{-1}) during winter season at (e) 500 m and (f) 1000 m depth

at subsurface levels. The sea surface topography plays the major role in the dynamics of circulation at subsurface levels. The westward flowing subsurface SEC has become more zonal at this depth as compared to its pattern at the surface and flows between the latitudes 10°S and 20°S. As noted at the surface, part of subsurface SEC turn towards north on reaching the east coast of Madagascar and joins with EACC. The southward flowing SC is still very strong at 50 m depth along the Somali coast and it joins with EACC to feed the subsurface eastward flowing Equatorial Under Current (EUC). The eastward flowing EUC is mainly driven by the east-west pressure gradient that exist between the latitudinal belt 0 - 10°N. A strong anti-clockwise gyre was observed off the Somali and East African coast at 50 m depth which is mainly caused by the peculiar sea surface topography pattern; in addition, a strong northward flow originating from the EUC was also observed at 50 m depth. In the northern Arabian Sea north of 10°N latitude, the flow pattern is now reversed, with eastward and northeastward flows seen in the entire northern Arabian Sea. This flow pattern is consistent with the sea surface topography pattern presented in Fig. 12. The sea surface topography slopes downwards towards north in the Arabian Sea and it would generate geostrophic flows directed towards east and northeast. In general, the model has been successful in reproducing all the permanent current systems in the western tropical Indian Ocean at 50 m depth, mainly the subsurface SEC, EACC, SC and EUC.

The winter mean current at 150 and 300 m depths are presented in Figs. 13 (c & d) respectively. The magnitude of current is considerably reduced in the northern Arabian Sea at both these depths where the average current speed is of the order of 5 to 10 cm sec^{-1}. In addition, weak clockwise and anticlockwise circulation cells have been found at these depths in the northern Arabian Sea. Two anticyclonic eddies are observed in the Arabian Sea at 150 m depth of which one is the well known Soccotra eddy located off the Soccotra islands. The second larger anticyclonic eddy is located in the eastern Arabian Sea east of 60°E longitude. The current along the Somali coast is now reversed and it flows towards south from 7.5°N latitude. The EUC could be seen in both the levels, but it moved slighly towards north and flows between the latitudes 2.5°N and 5°S. In the southern tropical Indian Ocean, the Mozambique Current (MZC) that flows westward and southwestward along the southern hemispheric Africa is also seen at 150 and 300 m depths. the westward flowing subsurface SEC flows between the latitudes 10°S and 20°S. The strength of SEC varies between 5 cm sec^{-1} and 10 cm sec^{-1}. At 300 m depth, a small clockwise eddy is found off the African coast between the equator and 5°S latitude.

The winter mean current at 500 and 1000 m depths are presented in Figs. 13 (e & f) respectively. The magnitude of flow field is further reduced at these depths as compared to upper levels and its speed varies between 7 cm sec^{-1} and 3 cm sec^{-1}. The Soccotra eddy found in the upper levels could be seen in both 500 and 1000 m depths. The circulation

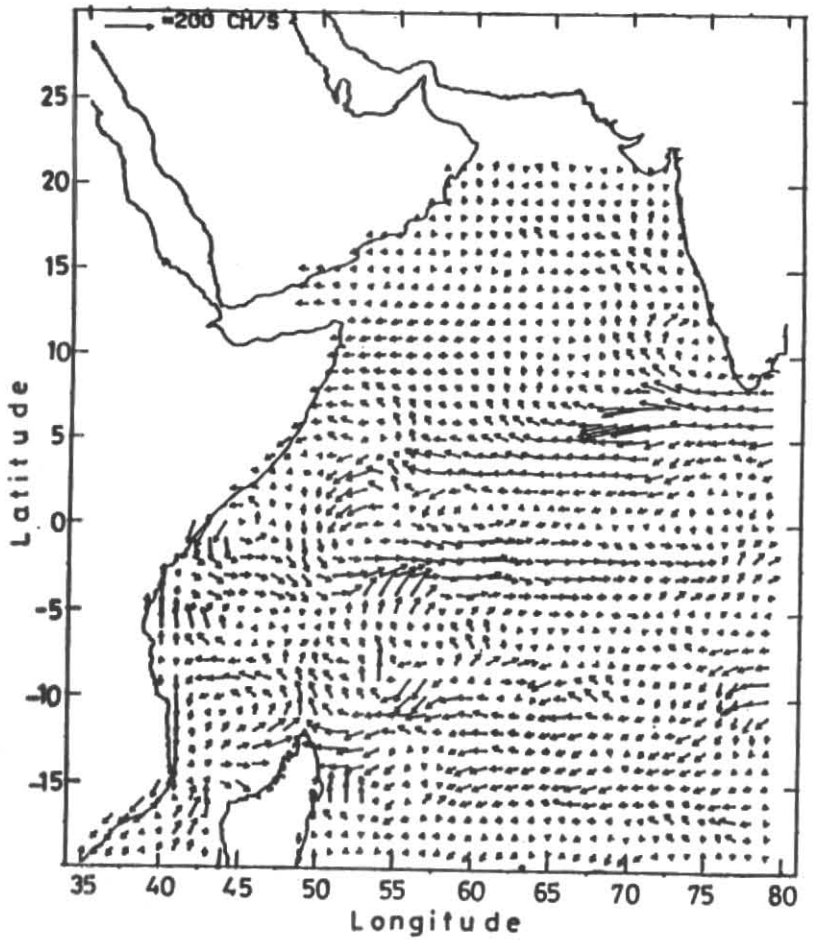

Fig. 14. The ship drift surface current of Cutler and Swallow (1984) during January

pattern in the southern tropical Indian Ocean is almost identical to what is observed in the upper levels, except that the magnitude of circulation is reduced.

4. Conclusion

A multi-level semi-diagnostic (adaptation) model of circulation was used to compute the summer and winter mean circulation in the western tropical Indian Ocean. The spin up time of the model is very fast as compared to prognostic ocean models and the soloution attains stationarity within 60 days of model ingtegration. The steady state solution shows that model is successful in reproducing all the permanent current systems in the tropical Indian Ocean which are mainly controlled by the local forcing of surface wind, density and sea surface topography. The computed anomaly fields for temperature and salinity at selected depths during the summer shows that the observed temperature and salinity data were adapted with surface wind, flow field and bottom relief and that the observed data were found to be fully smoothed during the adaptation stages. Semi-diagnostic technique is an effective tool to study the climatological circulation and also for the smoothing of climatological temperature and salinity data.

References

Bahulayan N. and Shaji,C., 1996, "Diagnostic model of 3-D circulataion in the Arabian Sea and western equatorial Indian Ocean: simulation results of sea surface topography", *Proc. Ind. Nat. Sci. Acad. (Physical Sciences).*, **62A,** 325-347.

Cutler,A.N. and Swallow,J.C., 1984, "Surface currents of the Indian Ocean", Institute of Oceanographic Sciences,U.K.,Report No.187,8p, 36 charts.\

Demin,Yu.L. and Ibraev,R.A., 1989, "A numerical method of calculation of currents and sea surface topography in multiply connected domains of the ocean", *Sov.J.Numer.Anal.Math.Modelling,* 4,3,211-225.

Gill,A.E., 1982, "Atmospheric-Ocean Dynamics", Academic Press,New York.,662 p.

Hellerman,S. and Rosenstein,M., 1983, "Normal monthly wind stress over the world ocean with error estimates", *J.Phys.Oceanogr.*, **13**,7,1093-1104.

Jensen,T.G., 1991, "Modelling the seasonal undercurrents in the Somali Current system", *J.Geophys.Res.*,**96**,22151-22167.

Levitus,S., 1982, "Climatological atlas of the world ocean", NOAA prof. paper 13,US Government Printing Office, Washington D.C., 173 p.

Luyten,J.R. and Roemmiah,D.H., 1982, "Equatorial currents at semi-annual period in the Indian Ocean", *J.Phys.Oceanogr.*,**12**,406- 413.

Marchuk,G.I. and Sarkisyan,A.S., 1988, "Mathematical modelling of ocean circulation", Springer-Verlag,Berlin, 292p.

McCreary,J.P.,Kundu,P.K. and Molinari,R.L., 1993, "A numerical investigation of dynamics, thermodynamics and mixed-layer processes in the Indian Ocean", *Progr.Oceanogr.*,**31**, 181-244.

Perigaud,C. and Delecluse,P., 1992, "Annual sea level variations in the tropical Indian Ocean from GEOSAT and shallow water simulations", *J. Geophys. Res.*,**97**,C12,20169-20178.

Quadfasel,D.R. and Schott,F., 1983, "Southward subsurface flow below the Somali Current", *J.Geophys.Res.*,**88**,C10,5973-5979.

Sarkisyan,A.S. and Demin, Yu.L., 1983, "Semi-diagnostic method of sea current calculation", Large scale oceanographic experiments in the WCRP publication series, Tokyo., **2(1)**,201-214.

Swallow,J.C.,Molinari,R.L.,Bruce,J.G. and Evans., R.H., 1983, "Development of near-surface flow pattern and watermass distribution in the Somali basin in response to the southwest monsoon of 1979", *J.Phys.Oceanogr.*,**13**, 1398-1415.

Wyrtki,K., 1973, "An equatorial jet in the Indian Ocean", *Science.*, **181**,262-264.